Nanomechanics of polymer gels and biological tissues: A critical review of analytical approaches in the Hertzian regime and beyond

David C. Lin* and Ferenc Horkay*

Received 21st September 2007, Accepted 17th December 2007
First published as an Advance Article on the web 5th February 2008
DOI: 10.1039/b714637j

We survey recent progress in the application of nanoindentation to characterize the local mechanical properties of polymer gels and biological tissues. We review the theories, analytical models based thereon, and data processing techniques commonly used to determine elastic properties of these classes of materials by instrumented nanoindentation. Examples from the testing of synthetic and biological gels are used to illustrate the limitations of existing theories and approaches. Emphasis is placed on the need for contact mechanics models that more accurately represent the large-strain behaviour of soft matter.

1. Introduction

With the advent of atomic force microscopy (AFM) and depth-sensing nanoindentation in the 1980s,[1,2] the measurement of local hardness and elastic properties by applying minuscule forces to probes of submicron dimensions became feasible. Sensitivity and resolution of the instruments have increased concomitantly with advances in miniaturization-enabling technologies such as photodetection, electrostatic and piezoelectric actuation, and microfabrication. Today, the AFM is a versatile tool for applications as diverse as atomic-resolution imaging[3] and force spectroscopy of inter- and intra-molecular interactions[4–6] while the mechanical characterization capabilities of both the AFM and the depth-sensing nanoindenter have been extended to include specialized functions such as wear and scratch testing and lateral force spectroscopy.[7,8]

Laboratory of Integrative and Medical Biophysics, National Institutes of Health, Bethesda, MD, 20892, USA. E-mail: lindavid@mail.nih.gov; horkay@helix.nih.gov

Conventional indentation, in which a rigid probe of well-defined geometry is pressed into the flat surface of a test sample by a force applied normal to the surface, is a well-established technique in the characterization of hard surfaces that undergo elastic–plastic deformation. Methods developed for macroscopic indentation have been shown to be transferable to micron and submicron length scales in the testing of many hard materials including metals, ceramics, plastics, calcified biological tissues, and composites.[9–13] When applied to soft materials that undergo purely elastic deformation even at large indentation depths, the physics of the indentation process are inherently more complex. Manifestations and consequences of the increased complexity include:

- Tip–sample interactions such as adhesion are generally stronger in compliant samples, particularly in tip retraction. Data analysis is therefore usually more difficult and may require models that provide for contributions from interactive forces.
- Applied forces for a given indentation depth are much smaller in soft materials, making the point of contact difficult

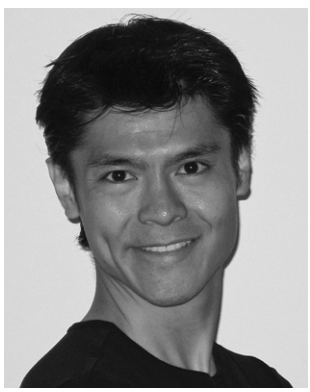

David C. Lin received his PhD from Rutgers University, where he worked with Professor N. A. Langrana on the development of a DNA-crosslinked hydrogel with tunable properties. In 2005, he joined the National Institutes of Health as a post-doctoral fellow in the Section on Tissue Biophysics and Biomimetics. His research interests are in the areas of tissue and soft matter mechanics, tissue engineering, biopolymers, and theoretical mechanics.

Ferenc Horkay received his PhD (1978) from the Loránd Eötvös University (Budapest) and DSc from the Hungarian Academy of Sciences. Prior to joining the National Institutes of Health in 1999, he was a senior research scientist at the Corporate Research and Development Center of the General Electric Corporation (Schenectady, NY). His research interest is to understand the fundamental principles that govern molecular interactions and define structural hierarchy in complex synthetic and biopolymer systems, such as gels, self-assemblies and functional nanostructures.

to identify in many cases. Moreover, signal-to-noise ratios can be adversely affected.

• Although the elastic deformation range of soft materials is typically larger than that of hard materials, the transition from linear to nonlinear stress–strain behaviour may be ambiguous. The opposite is true of many hard engineering materials, which possess obvious yield points.

Despite the hindrances that cast uncertainty on its accuracy, nanoindentation remains an important tool in the study of soft materials. For example, the AFM's capability of concurrent topographical imaging and mechanical probing has been exploited to generate high-resolution elasticity maps of tissues and cells, and even to chart the spatiotemporal evolution of stiffness during cellular processes.[14,15] Nanoindentation is also one of a small number of techniques not limited by sample size; for example, elastic properties of single vesicles as small as 100 nm in diameter have been measured.[16] The adoption of combinatorial methods in the design of polymer gels for biomedical use (*e.g.* in soft contact lenses, drug delivery agents, and tissue engineering scaffolds) has engendered demand for high-throughput characterization techniques compatible with the large libraries of minute sample volumes that are produced.[17–19]

In this article, we focus on the theories and analytical models used in measuring the elastic properties of soft materials by conventional nanoindentation. Esoteric theories such as those pertaining to single molecule force spectroscopy and the indentation of shells will be excluded. The body of work on indentation theory has focused chiefly on axisymmetric indenters, especially those that are spherical in form. Although such probes are most conducive to accuracy and consistency in mechanical measurements,[20] their use is not always warranted in practice (*e.g.* when concurrently imaging and probing the compliance of a sample using the atomic force microscope). Hence, other geometric models are covered where they are available and deemed congruent with the objective of this review. We examine various approaches utilized by researchers and discuss the applicability and shortcomings of each. It should become clear to the reader that the full potential of the nanoindentation technique, particularly when utilizing the AFM, cannot be realized without further developments in contact mechanics theory and modelling.

The paper is organized as follows: we begin with a brief summary of the Hertz contact mechanics theory. We then present a synopsis of the theories that incorporate tip–sample adhesive forces, followed by those that correct for the effect of small sample thickness. Next, we briefly discuss tip–sample repulsion and a proposed strategy for its treatment. A section is devoted to the discussion of nonlinear elastic contact mechanics. A number of analytical approaches based on linear elastic models are then highlighted, with the salient features of each identified. Finally, we provide an illustrative example of the shortcomings of each method and emphasize the strength of a combined approach. A comprehensive scheme is of particular importance in the nanoindentation of materials with large local inhomogeneities such as biological tissues (Fig. 1) and polymer composites. As a consequence of variations in local structure, composition, surface charge, *etc.*, the indentation response of these materials can vary over length scales comparable to the resolution of the instruments.

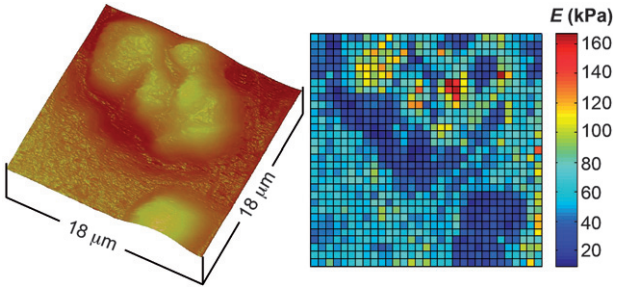

Fig. 1 (Left) AFM contact mode topography image of articular cartilage from the femoral head of a day-old mouse scanned over an 18 μm × 18 μm area with a sharp pyramidal tip. Raised regions are chondrocytes. (Right) Corresponding elastic modulus map of the same area at a resolution of 32 × 32 indentations using the same tip, showing the local inhomogeneities in stiffness. Note that the elastic modulus varies over two orders of magnitude.

2. Contact in the Hertzian regime

In reference to the original Hertz theory of contact between two elastic, ellipsoidal bodies[21] we define force–indentation behaviour that can be assumed to be governed by linear elasticity as being in the "Hertzian regime." Theories and models applicable in this range include those that account for influence from surface properties (*e.g.* tip–sample adhesion) and geometric factors (*e.g.* finite sample thickness).

2.1 Non-interactive indentation of an infinite half space

Hertz was the first to solve the problem of contact between two smooth, ellipsoidal solids.,[22] In the context of the indentation of a flat (infinite radius of curvature), elastic surface by a rigid sphere, the assumptions employed by Hertz can be summarized as follows:

• The strains are small, *i.e.* $a_c << R$, where a_c is the contact radius and R is the radius of the sphere.

• The indented solid is a linear elastic, infinite half space.

• The surfaces are frictionless.

Following Hertz's seminal treatise, numerous others (*e.g.* Boussinesq,[23] Love,[24] Segedin,[25] Landau and Lifshitz,[26] and Sneddon[27]) made significant contributions to the theoretical framework. Exact solutions in the form of force–indentation relationships, contact pressure distributions, and stress and displacement fields are readily available for common axisymmetric geometries (*e.g.* cone, cylinder, sphere) while approximate solutions have been derived for other geometries of practical interest such as sharp[28,29] and blunt[29] pyramids and blunt cones.[30,31] Force–indentation and contact radius relationships for the most common geometries are summarized in Table 1. In addition to uncertainties about their true geometric dimensions, the small tip angles of common tapered tips used in instrumented nanoindentation raise concerns of exceeding the linear stress–strain limit of the indented material.[20,28] Hence, care should be exercised to select probes of the largest available tip angle and to minimize indentation depths whenever possible.

2.2 Adhesive indentation of an infinite half space

Some degree of tip–sample interaction is often unavoidable in nanoindentation, with the type and magnitude of the force

Table 1 Indentation relationships for common indenter shapes

Model	λ^a	η	a_c (contact radius)
Hertz: sphere of radius R	$E^*R^{1/2}$	3/2	$(R\delta)^{1/2}$
Flat cylinder of radius r	$3E^*r/2$	1	r
Sharp cone of tip angle 2ϕ	$3E^*\tan\phi/(2\pi)$	2	$2\delta\tan\phi/\pi$
Sharp pyramid of face incline angle $\pi/2-\phi$, Bilodeau solution[b]	$3(1.4906)E^*\tan\phi/8$	2	$1.579^{1/2}\delta\tan\phi/2$
Sharp pyramid, Rico *et al.* solution[c]	$3E^*\tan\phi/2^{5/2}$	2	$\delta\tan\phi/2^{1/2}$
Blunt cone or blunt pyramid of tip angle 2ϕ, transitioning at radius or half-width b to round tip with radius R, with $b = R\cos\phi$	$F = \frac{3E^*}{2}\left\{a_c\delta - m\frac{a_c^2}{\tan\phi}\left[\frac{\pi}{2} - \arcsin\left(\frac{b}{a_c}\right)\right] - \frac{a_c^3}{3R} + \left(a_c^2 - b^2\right)^{1/2}\left[m\frac{b}{\tan\phi} + \frac{a_c^2 - b^2}{3R}\right]\right\}$ $\delta + \frac{a_c}{R}\left[\left(a_c^2 - b^2\right)^{1/2} - a\right] - n\frac{a_c}{\tan\phi}\left[\frac{\pi}{2} - \arcsin\left(\frac{b}{a_c}\right)\right] = 0$ cone : $m = 1/2, n = 1$ pyramid : $m = 2^{1/2}, n = 2^{3/2}/\pi$		

[a] $E^* = 4E/3(1-\nu^2)$ where E is Young's modulus and ν is Poisson's ratio. [b] Contact radius is actually half the length of one side of the square of contact. [c] Effective contact radius is of a circle with equal contact area.
General force–indentation relationship: $F = \lambda\delta^\eta$. F: force; δ : indentation depth; λ: geometry-dependent elastic constant; η: geometry-dependent exponent

affected by the composition and surface chemistry of the tip. Selecting the tip material or modifying its surface to be compatible with a specific sample is generally impractical. Hence, it is preferable to incorporate interactive interactions into contact mechanics theory. This was pioneered by Johnson *et al.*[32] who were motivated by the large body of evidence (usually manifested in enlarged contact area at a given load) suggesting the existence of attractive forces between both contacting hard and rubber-like solids. The JKR (Johnson–Kendall–Roberts) theory modifies the Hertz theory by introducing an apparent Hertz load, or the equivalent load in the absence of adhesion that produces the enlarged contact area. Later, Derjaguin *et al.*,[33] proposed the seemingly contradictory DMT (Derjaguin–Muller–Toporov) theory in which the deformed surface profile is assumed to follow the Hertz model. The ensuing debate persisted in the pages of the *Journal of Colloid and Interface Science*[34] until Tabor identified the applicability of the two theories to opposite extremes of the relationship between sample compliance and the range of the adhesive force.[35] The JKR theory was found to be valid for the indentation of relatively compliant materials with probes of relatively large radii and strong adhesive forces. In contrast, the DMT theory applies under conditions of stiff materials, small probe radii, and weak adhesive forces.

An important development in adhesive contact mechanics was advanced by Maugis,[36] who employed the Dugdale square-well approximation of the Lennard-Jones potential to formulate a closed-form solution to the general spherical indentation problem spanning the JKR and DMT limits. The Maugis–Dugdale theory consists of three equations that give an indirect relationship between force and indentation.[36,37] Carpick *et al.*[38] and Pietrement and Troyon[37] developed an empirical form of the theory that greatly enhances its practicality. The following set of equations comprises the empirical Maugis–Dugdale model:[37,38]

$$\delta = \frac{a_{c0}^2}{R}\left\{\left[\frac{\xi + (1 + F_n/F_{ad})^{1/2}}{1+\xi}\right]^{4/3} - S\left[\frac{\xi + (1 + F_n/F_{ad})^{2\beta/3}}{1+\xi}\right]\right\} \quad (1)$$

$$\frac{a_c}{a_{c0}} = \left[\frac{\xi + (1 + F_n/F_{ad})^{1/2}}{1+\xi}\right]^{2/3} \quad (2)$$

$$\bar{a}_{c0} = -0.451\xi^4 + 1.417\xi^3 - 1.365\xi^2 + 0.950\xi + 1.264 \quad (3)$$

$$\bar{F}_{ad} = 0.267\xi^2 - 0.767\xi + 2.000 \quad (4)$$

$$S = -2.160\xi^{0.019} + 2.7531\xi^{0.064} + 0.073\xi^{1.919} \quad (5)$$

$$\beta = 0.516\xi^4 - 0.683\xi^3 + 0.235\xi^2 + 0.429\xi \quad (6)$$

$$\bar{a}_{c0} = a_{c0}\left(\frac{3E^*}{\pi\gamma R^2}\right)^{1/3} \quad (7)$$

$$\bar{F}_{ad} = F_{ad}/(\pi\gamma R) \quad (8)$$

where δ is the indentation depth, a_{c0} is the contact radius at zero applied force ($F_n = 0$, corresponding to the point indicated by □ in Fig. 2), F_{ad} is the constant adhesive force (in Fig. 2, it can be seen that contact or separation occurs when $F_n = -F_{ad}$), γ is the interfacial energy, $E^* = 4E/3(1-\nu^2)$ where E is Young's modulus and ν is Poisson's ratio, ξ is a nondimensional parameter that represents the intermediacy within the JKR–DMT transition, S and β are nondimensional functions of ξ, and $\bar{a}_{c0}$ and $\bar{F}_{ad}$ are nondimensionalized equivalents of a_{c0} and F_{ad}. The special case $\xi = S = \beta = 0$ corresponds to the DMT theory while the JKR equations are recovered when $\xi = 1$ (and hence, $S = 2/3$

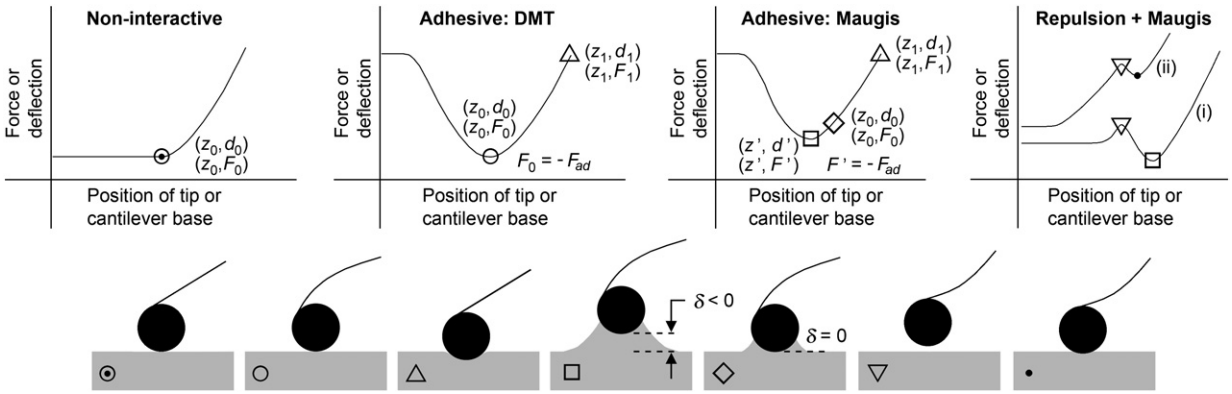

Fig. 2 Essential reference points for cases of non-interactive and adhesive indentation. Bending of the AFM cantilever at each point is shown. Raw data from the depth-sensing nanoindenter are usually in the form of force (F) *vs.* tip position. For the AFM, raw data are in the form of cantilever deflection (d) *vs.* position of the cantilever base. Tip position and base displacement are mathematically equivalent and designated by coordinate z. Indentation is always zero at the point of contact in the non-interactive (indicated by ⊙) and DMT (indicated by ○) models, but can be negative in the general case of adhesion (indicated by □) to allow for deflection of the sample surface towards the tip. The general case therefore additionally requires the point of zero indentation (indicated by ◇). The point of zero applied force (indicated by △) occurs at positive indentation depth for all cases of adhesion. Figure adapted from Lin *et al.*[50] When electrostatic repulsion at larger separation transitions to adhesion, the resulting response is dependent on whether the adhesive force is greater than (curve "i") or less than (curve "ii") the maximum repulsive force. In curve "ii" analysis should be performed using data subsequent to the point of contact (indicated by •).

and $\beta = 1/2$). It is worth noting that the "jump to contact" phenomenon observed in some instances of strong adhesion is consistent with the JKR theory, which predicts abrupt contact of $a_c > 0$ at the critical point where $F_n = -F_{ad}$.

The JKR theory was extended by Sun *et al.*[39] to a hyperboloid or blunt conical indenter of tip radius R and semivertical angle ϕ. The contact equations are:

$$\delta = \frac{a_c}{2\tan\phi}\left[\frac{\pi}{2} + \arcsin\frac{(a_c\tan\phi/R)^2 - 1}{(a_c\tan\phi/R)^2 + 1}\right] - \left(\frac{8\pi a_c\gamma}{3E^*}\right)^{1/2} \quad (9)$$

$$F_n = \frac{3E^*}{2}\left\{\frac{1}{2\tan\phi}\left[\frac{a_c R}{\tan\phi} + \frac{{a_c}^2 - R^2\cot^2\phi}{2}\left(\frac{\pi}{2} + \arcsin\frac{(a_c\tan\phi/R)^2 - 1}{(a_c\tan\phi/R)^2 + 1}\right)\right] - a_c\left(\frac{8\pi a_c\gamma}{3E^*}\right)^{1/2}\right\} \quad (10)$$

2.3 Non-interactive indentation of thin layers

The Hertz assumption of infinitesimal deformation (*i.e.* the indented sample is regarded as an infinite half-space) is a valid approximation in most practical applications. However, there exists a threshold in the ratio of maximum indentation depth to sample thickness at which errors from finite size effects become unacceptably large. Dimitriadis *et al.*[20] cited examples of corrections based on extensive numerical computations and found that Chadwick's approach provides a suitable estimate for modelling the indentation of very thin, incompressible layers by a spherical probe.[40] They prescribed a condition of $\chi = (R\delta)^{1/2}/h \leq 1$, where h is the sample thickness, for which their force–indentation relationship is valid:

$$F = E * R^{1/2}\delta^{3/2}\left[1 - \frac{2\psi}{\pi}\chi + \frac{4\psi^2}{\pi^2}\chi^2 - \frac{8}{\pi^3}\left(\psi^3 + \frac{4\pi^2}{15}\zeta\right)\chi^3 + \frac{16\psi}{\pi^4}\left(\psi^3 + \frac{3\pi^2}{5}\zeta\right)\chi^3\right] \quad (11)$$

In eqn (11), ψ and ζ are functions of Poisson's ratio and take on different forms based on the interfacial conditions between the sample and the underlying rigid substrate. When the sample is not bonded to the substrate, the parameters are given by

$$\psi = -0.347\frac{3-2\nu}{1-\nu}, \quad \zeta = 0.056\frac{5-2\nu}{1-\nu} \quad (12)$$

and when the sample is bonded to the substrate, they are given by

$$\psi = -\frac{1.2876 - 1.4678\nu + 1.3442\nu^2}{1-\nu}, \quad \zeta = \frac{0.6387 - 1.0277\nu + 1.5164\nu^2}{1-\nu} \quad (13)$$

For very thin incompressible samples (*i.e.* $\chi > 1$ and $\nu = 0.5$), use of Chadwick's solution is recommended:

$$F = (2\pi/3)ER^{1/2}\delta^{3/2}\chi^3 \text{ (bonded sample)} \quad (14)$$

$$F = (2\pi/3)ER^{1/2}\delta^{3/2}\chi \text{ (nonbonded sample)} \quad (15)$$

2.4 Repulsive tip–sample interactions

While adhesion is the most prevalent form of tip–sample interaction in the indentation of soft materials, other types of interactions are possible. Of particular interest is the existence of electrostatic forces when indentation is performed in aqueous

media, specifically in the presence of ions.[41] Models based on electrosteric and electrostatic interactions[41–43] and on the Derjaguin–Landau–Verway–Overbeek (DLVO) theory[44,45] have been applied in the limited body of work utilizing probe microscopy to measure the repulsive force between a probe and a flat surface. The majority of recent research efforts have focused on repulsive interactions between microbes and various materials.[46–49] These studies are concerned with surface properties of the investigated materials rather than their bulk mechanical properties. Hence, although the repulsive force between a probe and sample surface of like charge can be modelled as a function of the separation distance using the electrosteric, electrostatic, and DLVO models, force–indentation relationships that account for repulsion are lacking.

Lin *et al.*[50] proposed a simplistic and inexact approach to handling repulsive interactions in the contact regime. Similar to the treatment of adhesive forces in the JKR, DMT, and Maugis–Dugdale theories (see section 2.2), the maximum repulsive force is assumed to be constant at sufficiently large indentation depths. Consequently, the force–indentation relationship in this portion of the post-contact regime is offset from its zero-force position by a distance corresponding to the repulsive force. Because the mechanics in this region are otherwise assumed to be unchanged from the non-interactive case, the relationships in Table 1 along with eqn (11) – (15) are valid.

In rare cases, a more complex phenomenon can occur in which the electrostatic repulsion that dominates at larger separation distances is overcome by adhesive forces upon tip approach, resulting in the characteristic dip shown by curves "i" and "ii" in Fig. 2.[41] When the adhesive force is greater than the maximum repulsive force (curve "i"), the indentation mechanics are similar to those associated with pure adhesion, and can be analyzed as such. If, however, the adhesive force is less than the repulsive force (curve "ii"), the adhesive models are not applicable because the net force is repulsive at the point of contact. In this case, the suggested course of action is to discard the portion of data prior to contact and use the method outlined in the previous paragraph.

3. Contact beyond the Hertzian regime

In soft materials, the linear stress–strain approximation becomes progressively inadequate with increasing deformation. The strain at which deviation from linearity becomes significant is a material property that is seldom known prior to performing indentation experiments. Hence, it may be difficult to limit deformations to the linear regime. The lack of closed form force–indentation relationships appropriate for nonlinear elastic deformation has been the impetus for investigators to conduct numerical studies of nonlinear contact mechanics.[30,51] These studies illustrate the potentially significant errors that can be incurred by applying linear models to the indentation of stiffening or softening materials. The prevalence of using tapered tips to measure the mechanical properties of soft materials, particularly of cells and tissues, underscores the necessity for nonlinear contact mechanics models that cover a range of tip geometries and non-Hertzian deformations.

A number of phenomenological theories originating from polymer science have been developed over the years to describe the nonlinear elastic behaviour of rubbers and other polymeric materials.[52,53] Continued research in the nonlinear elasticity of soft materials now encompasses constitutive equations formulated to model the micromechanics of cells.[31,54,55] Such models, however, are largely academic except when implemented in computational methods. Interestingly, Jaasma *et al.*[56] found the indentation of osteoblasts with a spherical probe to closely follow a single parameter, second-order power law as a function of force.

Because contact mechanics remains a relatively underdeveloped field, linear models often serve as the basis for qualitative analyses of deformations beyond the Hertzian regime. For example, Costa *et al.*[57] used a pointwise approach of calculating Young's modulus with the blunt cone model (Table 1) to determine the extent of material nonlinearity. By comparing the value of E at each point, the stiffening and softening behaviour could be discerned. Mathur *et al.*[58] observed similar transitions in the elastic modulus with indentation depth in their studies on cardiac and skeletal muscle cells.

Lin *et al.*[59] addressed the dearth of nonlinear force–indentation relationships and derived an approximate equation based on the Mooney–Rivlin strain energy function.[53] The relationship for the indentation of a rubber-like material by a rigid sphere of radius R is

$$F = \pi R^{1/2} B_1 \left(\frac{\delta^{5/2} - 3R^{1/2}\delta^2 + 3R\delta^{3/2}}{\delta - 2R^{1/2}\delta^{1/2} + R} \right) + \pi R^{1/2} B_2 \left(\frac{R^{1/2}\delta^{5/2} - 3R\delta^2 + 3R^{3/2}\delta^{3/2}}{-\delta^{3/2} + 3R^{1/2}\delta - 3R\delta^{1/2} + R^{3/2}} \right) \quad (16)$$

where B_1 and B_2 are essentially the Mooney–Rivlin constants and are related to Young's modulus at infinitesimal strain, E_0, by[59]

$$B_1 + B_2 = \frac{4E_0}{9\pi(1-\nu^2)} \quad (17)$$

The net force is equal to the sum of the applied force and the adhesive force ($F = F_n + F_{ad}$) if adhesion is present and conforms to the specific conditions of the DMT theory (stiff material, small probe radius, and weak adhesive force). However, eqn (16) cannot be used for general cases of adhesion. The model reduces to the neo-Hookean form[53] when $B_2 = 0$. Although the neo-Hookean equation should be adequate for perfectly rubber-like materials under compression, Lin *et al.* suggested the use of the Mooney–Rivlin form to allow for slight deviations from rubber elastic behaviour. Eqn (16) eliminates the need to limit deformations to the linear regime or to truncate datasets, and was shown to be a good fit for the large-strain indentation of swollen poly(vinyl alcohol) gels and some cartilage samples.[59] The method of derivation of eqn (16) can be extended to other hyperelastic strain energy potentials (*e.g.* Ogden, van der Waals, Fung).[60,61] The family of equations thus generated covers models that have been used successfully for many rubber-like gels and soft tissues.

4. Analytical techniques

A multitude of techniques have been developed for the analysis of data from the AFM or depth-sensing nanoindenter. Virtually all the techniques presented in this section were designed for

extracting linear elastic properties from indentation data. Many, however, can be adapted for use with eqn (16). The features, capabilities, and shortcomings of what we believe to be the most representative approaches will be discussed. We will assess the capability of each in handling irregular data sets (*i.e.* those with excessive noise, significant adhesion, or significant repulsion). Obviously, it is not possible to cover the intricacies of implementing each technique. However, it is hoped that this critical review will aid the researcher in selecting or developing an approach suitable for the analysis of experimental data.

Before commencing with the survey of methods, the subject of material compressibility merits a brief discussion. While the assumption of sample incompressibility applied in many tests is generally valid, Poisson's ratio of some materials, particularly soft tissues, can be significantly less than 0.5. Using the Hertz equation as an example, it can be verified that the assumption results in an underestimation of Young's modulus by nearly 18% and 11% for actual Poisson's ratios of 0.3 and 0.4, respectively. In the following methods, if Poisson's ratio is unknown, it can be combined with Young's modulus to form an effective material constant (*e.g.* E^* in Table 1) useful for comparing the elasticity of materials with similar compressibility. Note, however, that the quantity is not as meaningful as Young's modulus.

4.1 Reference point dependence

The majority of methods require the determination of reference points to transform positional coordinates to force and indentation data. The complexity of the process depends on whether adhesive interactions are present and on the type of instrument employed, with the depth-sensing systems generally requiring less rigorous treatment of the raw data due to their ability to measure forces directly. For typical AFM and depth-sensing nanoindenter setups, the essential reference points under non-interactive and adhesive conditions as identified by Lin *et al.*[50] are summarized in Table 2 and illustrated in Fig. 2. Force and indentation depth are derived from the reference points using the relationships listed in Table 3.

Table 2 Essential reference points in nanoindentation data processing

Instrument type	Non-interactive Indentation	Adhesive Indentation[a]
Atomic force microscope	Contact or release/ zero indent: (z_0, d_0)	Contact or release: (z', d')
		Zero indent: (z_0, d_0)
		Zero force: (z_1, d_1)
Depth-sensing nanoindenter	Contact or release/zero indent: (z_0, F_0)	Contact or release: (z', F')
		Zero indent: (z_0, F_0)

[a] When adhesion is governed by the DMT theory, *i.e.* $\alpha = S = \beta = 0$ in eqn (1) – (8), the point of zero indentation is also the contact point.
z is the position of the tip (nanoindenter) or cantilever base (AFM).
d is the deflection of the cantilever (AFM).
F is the net force measured by the force actuator of the nanoindenter.

For non-interactive contact, the implications of an incorrectly identified contact point (equivalent to the release point in tip retraction) on the accuracy of extracted mechanical properties were studied by Crick and Yin.[62] Simulations were performed of the indentation of materials with linear and nonlinear stress–strain properties using a blunt conical tip. It was found that the errors incurred by misidentifying the contact point were affected by the linearity and stiffness of the material, the level of noise in the data, the distance of the misidentified point from the actual contact point, and whether the misidentified point was situated in the pre-contact or post-contact region.

4.2 Methods for non-adhesive contact

4.2.1 General principles of data fitting. Techniques based purely on data fitting are usually implemented in search strategies. The appropriate transformations in Table 3 are substituted into a force–indentation relationship to form the fitting equation; the sole reference point in non-adhesive indentation is the contact point. These methods were further grouped by Lin *et al.* according to whether the identified contact point is required to be a member of the data set.[63] Different levels of constraints were defined:

- Fully constrained, in which the contact point must come from the data set and the lone fitting parameter is an elastic constant.
- Semi-constrained, in which only one coordinate of the contact point is from the data set and the other coordinate along with an elastic constant are the fitting parameters. Bounds can be imposed on the parameters.
- Unconstrained, in which both coordinates are allowed to fall outside the data set, leaving three fitting parameters (both coordinates of the contact point and an elastic constant). A good initial guess of the contact point is usually necessary.

Variants of these search procedures have been used by many researchers to process data from the nanoindentation of hydrogels, cells and other biologically relevant materials.[14,20,29,64–68] The semi-constrained and unconstrained techniques help to compensate for errors arising from high levels of noise (*e.g.* ensuing from adhesive "jump to contact") or from relatively minor misidentifications of the contact point by allowing the

Table 3 Force and indentation relationships

Instrument type	Non-interactive Indentation	Adhesive Indentation
Atomic force microscope	$F = F_n = k_c(d - d_0)$	$F = F_n + F_{ad} = k_c(d - d_1) + k_c(d_0 - d_1)$
	$\delta = (z - z_0) - (d - d_0) = (z - d) - (z_0 - d_0) = w - w_0$	$\delta = (z - z_0) - (d - d_0) = (z - d) - (z_0 - d_0) = w - w_0$
Depth-sensing nanoindenter	$F = F_n = F - F_0$	$F = F_n + F_{ad} = (F - F_1) + (F_0 - F_1)$
	$\delta = z - z_0$	$\delta = z - z_0$

k_c is the spring constant of the cantilever; $w = z - d$ is a transformed position coordinate introduced for simplicity and w_0 is its value at the contact point.

contact point to "float". Ideally, multiple iterations are not necessary with the unconstrained technique. Lin *et al.* found the semi-constrained approach to be amenable to optimization strategies such as the Golden Section search, which offsets its relative computational expense.[63] This is illustrated in Fig. 3 by the plots of the fitting error as the assumed contact point is moved along the curves of three sample data sets.

Because the fitting schemes are compatible with any force-indentation equation, material nonlinearity does not preclude their use. In their large-strain AFM indentation tests of poly(vinyl alcohol) hydrogels and cartilage specimens, Lin *et al.*[59] applied eqn (16) successfully in an implementation of a semi-constrained search procedure. These schemes fail to produce acceptable fits of the data, however, when large repulsive forces obscure the contact point. As in the case of adhesion, the contact point is shifted under the influence of repulsive forces and non-interactive contact models do not accurately fit the data. By assuming the maximum repulsive force to be constant at sufficiently large indentation depths, Lin *et al.*[63] argued that the force–indentation behaviour essentially obeys non-interactive contact mechanics. Discarding the data points affected by repulsion, a semi-constrained "rearwards search" is performed to locate a surrogate contact point (see curve "c" in Fig. 3).

4.2.2 Method of Crick and Yin. As a complement to their study, Crick and Yin proposed an algorithm for finding the contact point and subsequently extracting the value of Young's modulus.[62] Using a moving subset containing 25% of all data points, the difference in cantilever deflection between the first and last points is used to evaluate whether the contact point is bracketed within the subset. The iterative process is performed until the difference is significantly greater than the noise level. The first and last points of the subset are then used to define initial lower and upper bounds of the search interval. The size of the interval is adjusted according to rough estimates of the stiffness of the material and the location of the contact point. Within the new interval, an exhaustive search is performed by fitting the first half of the data up to the candidate contact point with a line and the second half with either another line or a quadratic function. The solution is determined from an aggregate measure of the accuracy of each fit.

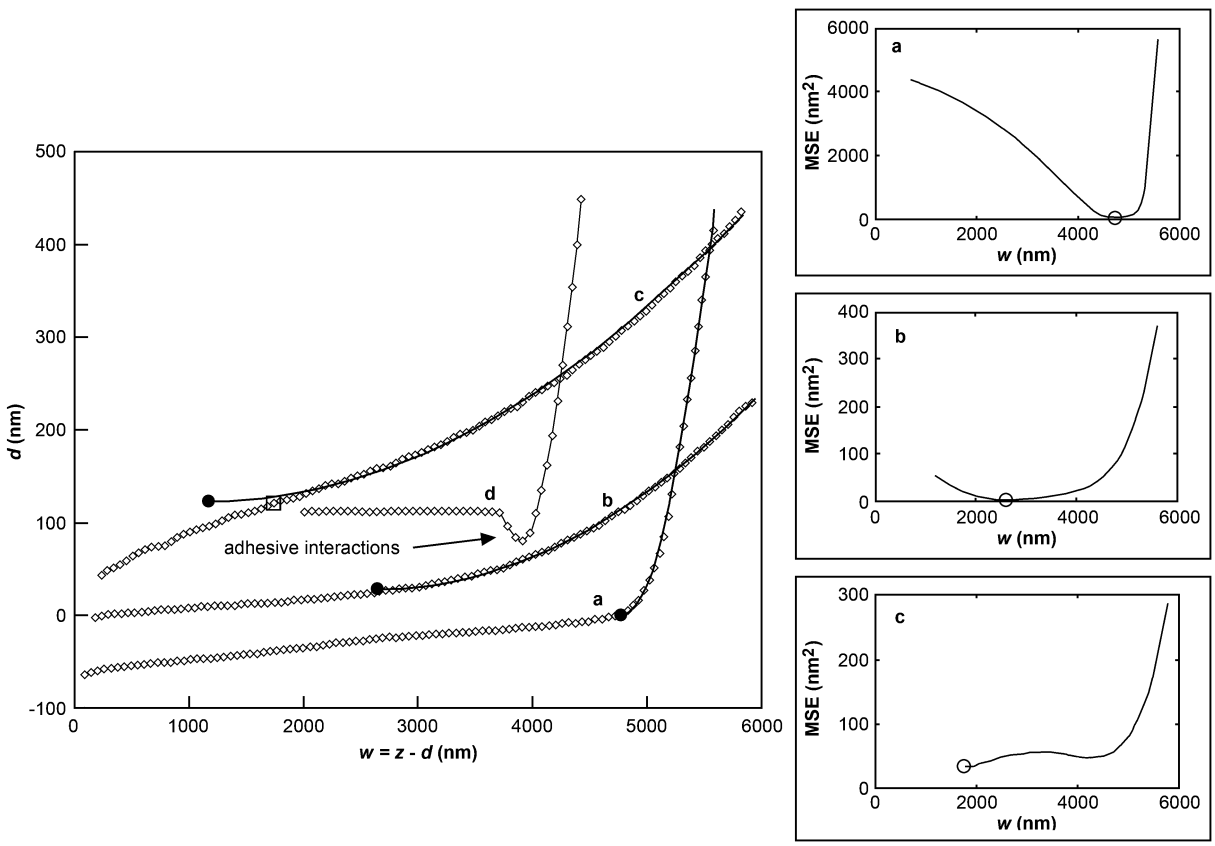

Fig. 3 Curves "a"–"c": Force curves (every fifth point indicated by ◇), best-fit curves (dark solid lines), and corresponding plots of the mean-square-error (MSE) as a function of the position of the assumed contact point using a linear, semi-constrained search. Three separate indentations of engineered cartilage specimens with a 9.6 μm diameter spherical tip are shown. For visualization purposes, curves were shifted vertically with no effect on the solutions. In curve "c", points prior to the inflection point (indicated by □) and presumably influenced by repulsive forces, were discarded from the analysis. A surrogate contact point (indicated by •) is found using a semi-constrained rearwards search. When the contact point lies within the range of the retained data, the MSE plot is unimodal (curves "a" and "b") and optimization strategies such as the Golden Section search can be implemented. When the contact point lies outside the range of the retained data (curve "c"), as is prone to occur with significant repulsion, the MSE plot does not have a global minimum. Curve "d" is a representative curve showing significant adhesive interactions, and requires a different analytical approach. Data from Lin *et al.*[50]

This method can be extended for nonlinear elastic indentation by substituting eqn (16) in place of the linear or quadratic functions for fitting the assumed contact portion of the data. Its chief deficiency is that it will only work when the pre-contact portion of the data set is virtually free from tip–sample interactions. Repulsion and adhesion may both cause the bracketing procedure to erroneously omit the true contact point from the search interval. It is clear that this is the case for sample data set "c" shown in Fig. 3, where the difference in deflection between the first and last points of any subset will be substantially larger than the level of noise.

4.2.3 Method of Jaasma *et al.*. For indentation in the Hertzian regime with a tip profile satisfying the general force–indentation relationship given in Table 1 ($F = \lambda\delta^{\eta}$), Jaasma *et al.*[56] showed that the derivative of the AFM cantilever deflection with respect to the base position is zero at the point of contact or release. This relationship is linear for their empirical value of $\eta = 2$. Extrapolation of post-contact portions of the data to the point of zero derivative yields the location of the point of contact or separation. Regression analysis is applied to determine Young's modulus. This method requires that the deformation be confined to the linear regime. However, it is compatible with adhesive and repulsive indentation provided that there is sufficient data at large indentation depths for which interactive forces are negligible. It is important to note that because the analysis is based on the derivative of the data, high levels of noise may introduce large errors.

4.2.4 Method of Guo and Akhremitchev. Guo and Akhremitchev[69] devised a data fitting scheme based on the linearization of data. The general force–indentation relationship given in Table 1 is first rewritten in terms of the tip–sample separation distance Δ and a constant C related to the point of contact or separation ($\delta = C - \Delta$, where δ is the indentation depth).[70] The linearization in Δ is obtained by rewriting the general equation as

$$F^{1/\eta} = C^{*} - \lambda^{1/\eta}\Delta \tag{18}$$

where C^{*} is another constant and equal to $\lambda^{1/\eta}C$.

Guo and Akhremitchev estimate a maximum systemic error of approximately 10% associated with manually selecting the point of contact or separation. This method is most suitable for data sets in which the point can be easily identified. After transforming the raw coordinates to values of force and indentation, points in the post-contact region are plotted using eqn (18). Young's modulus is then extracted from the slope of the line. Indentations are required to be linear elastic and non-interactive.

4.2.5 Method of Oliver and Pharr. This method is an extension of traditional methods for determining the hardness and elastic moduli of solid materials.[71] In order to limit experimental complexity and make the method more tractable for nanoindentation data, Oliver and Pharr dispensed with the need to measure the geometry of the residual impression. Hence, their approach can be adapted for the indentation of soft materials.[72–76]

For indentation with a rigid indenter, the reduced modulus, E_r, is defined by[71]

$$E_r = \frac{E}{1-\nu^2} = \frac{\sqrt{\pi}}{2}\frac{\sigma}{\sqrt{A_c}}$$

where σ is the initial loading stiffness determined from the derivative of the transformed force–indentation relationship at maximum load and A_c is the corresponding contact area. Although Oliver and Pharr performed experiments to establish the relation between the contact radius and applied load, the equations in Table 1 can be used in lieu of empirical relationships. Eqn (19) serves as a substitute of the regression analysis employed in other approaches of extracting the elastic modulus. The constraint of limiting the analysis to the unloading data can be relaxed in testing many soft materials due to the absence of inelasticity.

4.2.6 Method of A-Hassan *et al.*. A-Hassan *et al.*[77] proved that the relative work of indentation (*i.e.*, the ratio of areas under the force–indentation curves for two different samples) is proportional to the ratio of their stiffness. Hence, the work can be used as a relative measure of the elastic modulus. Although this method is valid for both linear and nonlinear deformation and does not require the identification of reference points, its practicality is severely limited by its inability to measure the absolute elastic moduli of materials.

4.2.7 Other methods. A number of other contact point dependent methods, mostly designed for non-interactive contact, have been described in the literature. We touch on a few of them here to provide awareness of alternative schemes:

- Derivatives of cantilever deflection[78] – the contact or release point is assumed to occur at the point of maximum change in deflection with respect to the cantilever base position. When the level of noise is high, however, large errors in the detected contact point are likely.
- Average deflection in the contact region[79] – after identifying the pre-contact portion of the data set, the average of the deflection is calculated. The force–indentation equation is then fit to the purported contact portion of the data, with the elastic constant and the z-coordinate of the contact or release point as fitting parameters. The pre-contact region will be difficult to identify unless tip–sample interactions are absent and the level of noise is low.
- Power series correction[80] – the force–indentation equation is expanded in a two-term power series about an arbitrary point in the vicinity of the contact or release point. This modified fitting equation is then used to find the values of the elastic constant and the coordinates of the true contact or release point. Subjectivity in the selection process and significant influence from the size of the pre-contact portion make this method difficult to implement.

4.3 Methods for adhesive contact

4.3.1 Method of Lin *et al.* for adhesive interactions. When adhesion is detected (see Fig. 2 and curve "d" in Fig. 3), typically in tip retraction, Lin *et al.*[81] proposed an approach based on the Pietrement–Troyon empirical model represented by eqn (1) – (8). The locations of the zero force and contact reference points

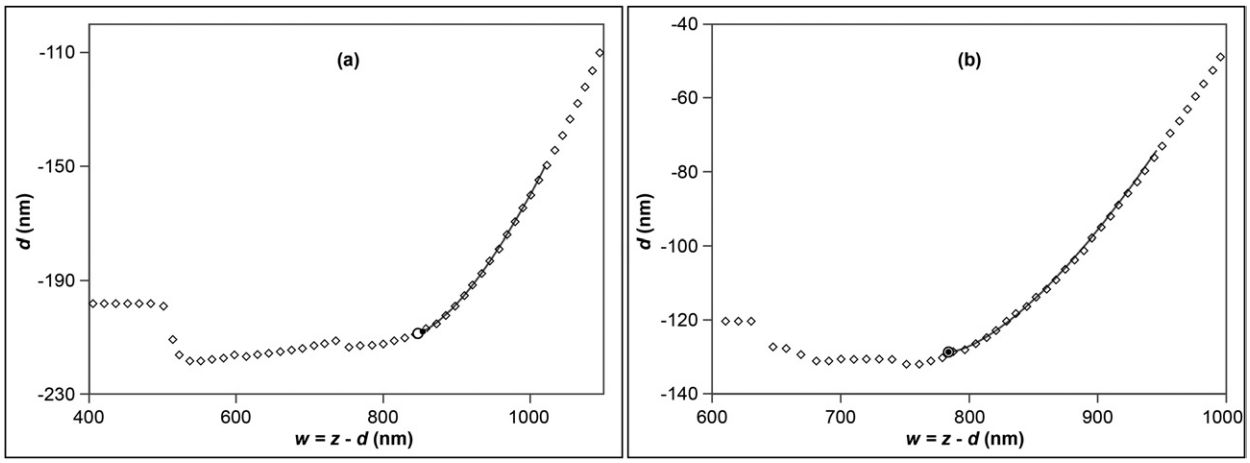

Fig. 4 Sample retraction curves from the AFM indentation of a poly(vinyl alcohol) gel using a 9.6 μm diameter spherical tip. The contact points (indicated by ○) and the zero indentation reference point (indicated by •) do not necessarily coincide. Data from Lin *et al.*[81]

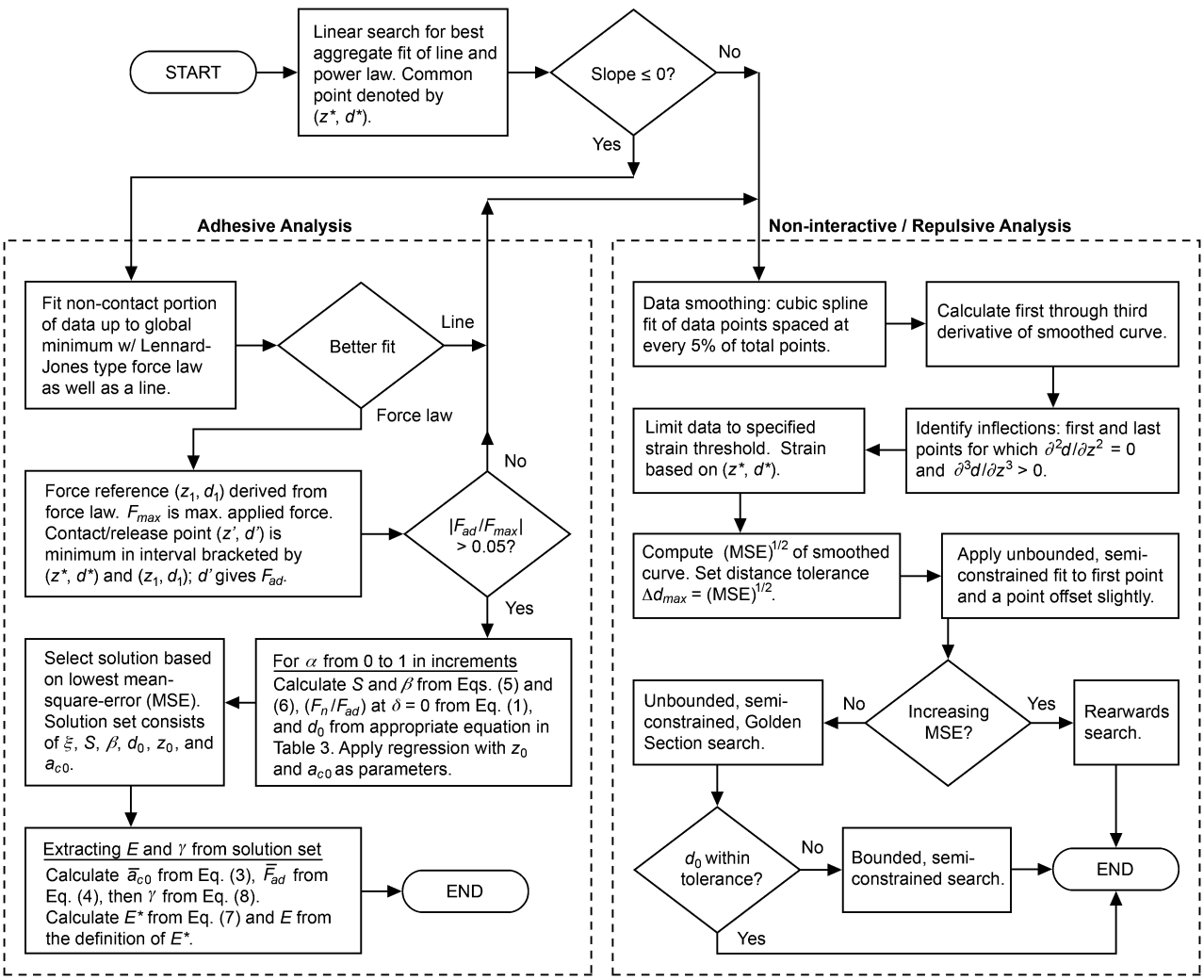

Fig. 5 Flowchart representation of the algorithm developed by Lin *et al.*[50] for the analysis of AFM nanoindentation data. Contingencies for repulsive and adhesive interactions are incorporated into the scheme.

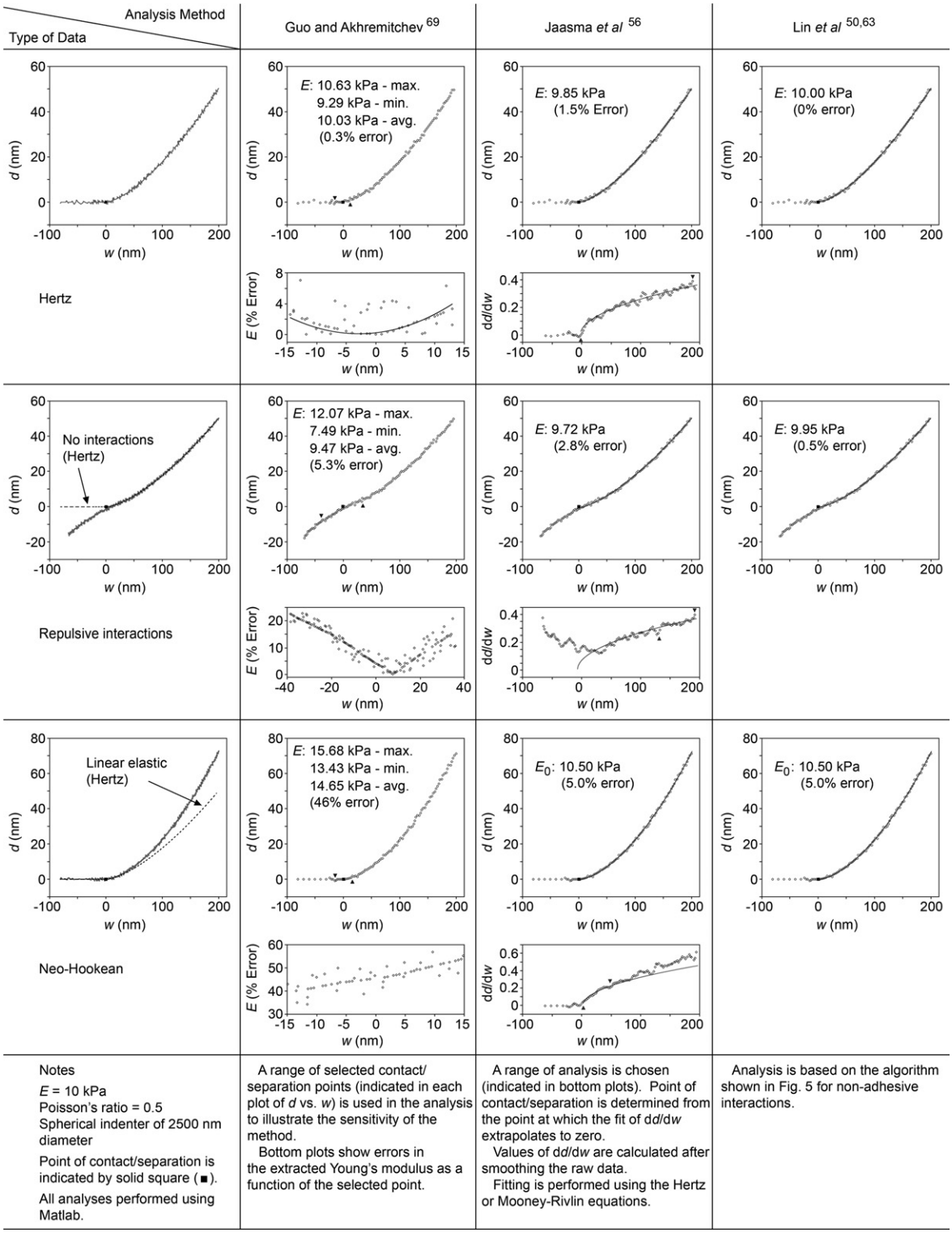

Fig. 6 Simulated, non-adhesive AFM data sets analyzed by three methods. Random noise of up to ±1 nm was added to each value of deflection *d*. For the method of Jaasma *et al.*[56] the range of analysis was found through trial and error. For the neo-Hookean data, the method of Guo and Akhremitchev[69] relies on the Hertz equation. For the Hertz and neo-Hookean data sets, the method of Crick and Yin[62] yields essentially the same results as the method of Lin *et al.*[50,63] Best-fit curves (solid lines) are plotted with the data (every fifth point indicated by ○) where possible.

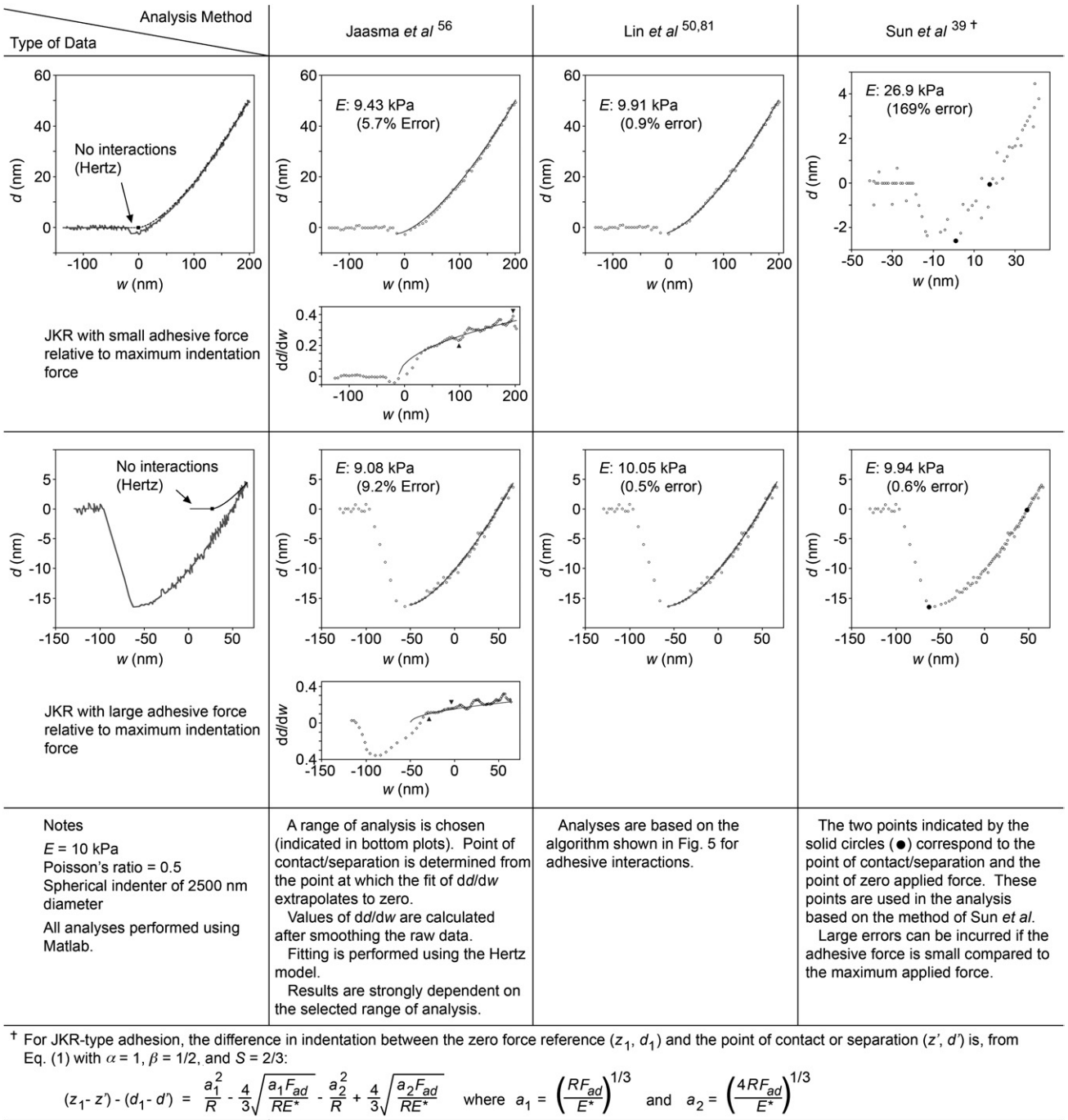

† For JKR-type adhesion, the difference in indentation between the zero force reference (z_1, d_1) and the point of contact or separation (z', d') is, from Eq. (1) with $\alpha = 1$, $\beta = 1/2$, and $S = 2/3$:

$$(z_1 - z') - (d_1 - d') = \frac{a_1^2}{R} - \frac{4}{3}\sqrt{\frac{a_1 F_{ad}}{RE^*}} - \frac{a_2^2}{R} + \frac{4}{3}\sqrt{\frac{a_2 F_{ad}}{RE^*}} \quad \text{where } a_1 = \left(\frac{RF_{ad}}{E^*}\right)^{1/3} \text{ and } a_2 = \left(\frac{4RF_{ad}}{E^*}\right)^{1/3}$$

Fig. 7 Simulated, JKR type adhesive AFM data sets analyzed by three methods. Best-fit curves (solid lines) are plotted with the data (every fifth point indicated by ○) where possible.

(Table 2 and Fig. 2) are determined independently prior to the principal data fitting and search process. The separation point (or contact point in the loading phase) is taken to be the point of minimum absolute deflection (*i.e.* the bottom of the valleys shown in Fig. 2) when the tip completely detaches from the sample upon initial release. Frequently in the indentation of soft materials, multiple release points resulting in a sawtooth pattern are observed.[81,82] Examples of this phenomenon can be seen in the two data sets displayed in Fig. 4. When this occurs, the first release point is chosen to be the reference point.

Following the identification of the first two reference points, an iterative search for the zero indentation reference point is conducted by varying the value of the nondimensional parameter α that represents the intermediacy within the JKR–DMT transition. At each iteration, eqn (1), (5) and (6) are used to calculate the coordinates of the reference point at $\delta = 0$. The coordinates that result in the best fit of the data are accepted as the solution. Young's modulus can be extracted from eqn (3), (4), (7) and (8). Because this method is based on an empirical form of the Maugis–Dugdale theory, it shares the same

Table 4 Matrix of methods, amount of user intervention required in implementing each method, and types of AFM data each is suited for

Data	Crick and Yin[62]	Guo and Akhremitchev[69]	Jaasma *et al.*[56]	Lin *et al.*[50,63,81]	Oliver and Pharr[71]	Sun *et al.*[39]
Non-interactive, Hertzian	✓	✓	✓	✓	✓	
Repulsive		✓[a]	✓[b]	✓		
Mooney–Rivlin elastic	✓		✓[b]	✓		
Small adhesive force	✓	✓[a]	✓[b]	✓	✓	
Large adhesive force of JKR type				✓		✓
Large adhesive force of DMT type				✓		✓
Large adhesive force in the JKR–DMT transition				✓		
User intervention	Minimal	Significant	Moderate	Minimal	Significant	Minimal

[a] Accuracy is contingent on the selected contact/separation point or range of points. [b] Accuracy is contingent on the range of data used in the analysis; a fixed range may not be suitable for all data sets.

limitations. These include the requirements of material linearity and large relative sample thickness.

4.3.2 Method of Sun *et al.* for adhesive interactions. An alternative technique for analyzing indentation data sets that are strongly influenced by adhesive interactions was developed by Sun *et al.*[39] using transformed force and indentation data. The zero force reference, which can generally be identified with little difficulty, and another reference point (*e.g.* the release point) are used to generate four equations based on eqn (1) and (2) or on eqn (9) and (10). This system of equations can be solved for the four unknown quantities (the contact radius at the two points, the interfacial energy, and the elastic constant E^*). Especially in the case of the AFM, however, transformation of the data may be difficult. In such circumstances, a single equation can be generated for the change in indentation between the two chosen reference points using eqn (1) or (9).

Because this method makes use of only data up to the zero force reference, material nonlinearity is not a concern. For spherical indenters, it should also be compatible with the JKR and DMT theories, but not the general Maugis–Dugdale theory. Care should be exercised to limit the indentation depth in order to minimize the amount of superfluous data. It should also be realized that because only two points are used in the analysis, the results depend greatly on the accuracy in identifying the reference points.

4.4 Combined approaches

Lin *et al.*[63] offered an algorithm as an example of combining multiple analysis strategies into a synergistic approach that can better handle different types of problematic data sets (*e.g.* excessive noise and tip–sample adhesion or repulsion). Two main conditions were stipulated as key requirements of a comprehensive scheme:

- It must be capable of detecting and handling data sets that are influenced by adhesion or repulsion.
- User intervention should be minimized to prevent subjectivity.

In the algorithm, a preprocessing step determines whether adhesive interactions are present and invokes one of two measures – one based on the semi-constrained search and the rearwards search procedure for non-interactive or repulsion-influenced data, and the other based on the empirical Pietrement–Troyon model for adhesive interactions. The algorithm is represented in flowchart form in Fig. 5.

If accuracy is the primary criterion in formulating an analytical approach, multiple techniques can be employed and their results compared to identify the best solution (*i.e.* the one that provides the best fit of the data). For example, the method of Jaasma *et al.*[56] can be used to identify the point of contact or separation, and then the method of Guo and Akhremitchev[69] can be applied to extract the value of Young's modulus from the transformed data. The advantages of applying a combined approach are illustrated in Fig. 6 and 7, where simulated data sets are analyzed using a number of methods. In Table 4, we identify the methods that are most suitable for various types of data as well as those that require minimal user input and hence, are most appropriate for automated analysis schemes. The comparisons should provide a clearer understanding of the capabilities of the different methods.

5. Conclusions and future perspectives

Nanoindentation of soft materials can present several unique challenges compared to the traditional processes developed for the testing of hard materials. The analytical approaches based on linear elasticity theory listed in this paper are all capable of accurately extracting elastic properties from ideal data sets that exhibit high signal-to-noise ratios, limit deformations to the Hertzian regime, and have conspicuous points of contact or separation. In intractable data sets, complications usually arise in the form of ambiguities in the location of important reference points. Under such circumstances, a combination of techniques is the recommended course of action.

When the deformations extend beyond the Hertzian regime, the linear elastic models are inadequate. In fact, the linear elastic limit may be essentially nonexistent in many materials of biological origin. Additionally, the nonlinear response may vary significantly among different materials. Although a simple force–indentation relationship based on the Mooney–Rivlin formalism has been developed and validated for the testing of certain gels and soft tissues, no hyperelastic model exists that is capable of serving as a universal constitutive law for soft elastic materials. Hence, multiple models are necessary for representing the diversity of large strain behaviours that exists among soft matter. It is obvious that further advances in the area of nonlinear elastic indentation modelling are required to match the rapid growth of nanoindentation in fields from polymer science to biology.

6. List of symbols

a_1 contact radius at point of contact or separation in JKR-type adhesive contact
a_2 contact radius at point of zero applied force in JKR-type adhesive contact
a_c contact radius
a_{c0} contact radius at zero applied force
$\bar{a}_{c0}$ nondimensionalized value of a_{c0} used in empirical Maugis–Dugdale model
A_c contact area
B_1 first Mooney–Rivlin or neo-Hookean elastic constant for spherical indentation
B_2 second Mooney–Rivlin elastic constant for spherical indentation
C constant used to relate indentation depth and separation distance in the method of Guo and Akhremitchev[69]
C^* constant obtained after linearizing the relationship between force and separation distance in the method of Guo and Akhremitchev[69]
E Young's modulus
E_r elastic constant or reduced modulus used in the method of Oliver and Pharr[71]
E^* elastic constant combining Young's modulus and Poisson's ratio
F net indentation force
F_{ad} adhesive force
$\bar{F}_{ad}$ nondimensionalized value of F_{ad} used in empirical Maugis–Dugdale model
F_n normal or externally applied force
k_c spring constant of AFM cantilever
R radius of spherical indenter
S nondimensional term used in the empirical Maugis–Dugdale model
β nondimensional term used in the empirical Maugis–Dugdale model
χ transformed indentation depth used in finite layer thickness models
δ indentation depth
Δ tip–sample separation distance
ϕ semivertical or half tip angle of conical or pyramidal indenter
γ interfacial energy
η geometry-dependent exponent in the general force–indentation equation
λ geometry-dependent elastic constant in the general force–indentation equation
ν Poisson's ratio
σ loading stiffness at maximum load during tip retraction
ξ nondimensional constant representing intermediacy within the DMT–JKR transition
ψ constant representing the interfacial condition between sample and underlying rigid substrate
ζ constant representing the interfacial condition between sample and underlying rigid substrate

7. Acknowledgement

This work was supported by the Intramural Research Program of the National Institutes of Health/National Institute of Child Health and Human Development.

8. References

1 G. Binnig, C. F. Quate and C. Gerber, *Phys. Rev. Lett.*, 1986, **56**, 930–933.
2 J. B. Pethica, R. Hutchings and W. C. Oliver, *Philos. Mag.*, 1983, **48**, 593–606.
3 F. J. Giessibl, *Rev. Mod. Phys.*, 2003, **75**, 949–983.
4 F. Kienberger, A. Ebner, H. J. Gruber and P. Hinterdorfer, *Acc. Chem. Res.*, 2006, **39**, 29–36.
5 C. K. Lee, Y. M. Wang, L. S. Huang and S. Lin, *Micron*, 2007, **38**, 446–461.
6 C. Ray, J. R. Brown and B. B. Akhremitchev, *J. Phys. Chem. B*, 2007, **111**, 1963–1974.
7 S. D. Kenny, D. Mulliah, C. F. Sanz-Navarro and R. Smith, *Philos. Trans. R. Soc. Lond., Ser. A*, 2005, **363**, 1949–1959.
8 E. Tocha, H. Schonherr and G. J. Vancso, *Langmuir*, 2006, **22**, 2340–2350.
9 B. J. Briscoe, L. Fiori and E. Pelillo, *J. Phys. D: Appl. Phys.*, 1998, **31**, 2395–2405.
10 G. Feng and A. H. W. Ngan, *J. Mater. Res.*, 2002, **17**, 660–668.
11 G. Pelled, K. Tai, D. Sheyn, Y. Zilberman, S. Kumbar, L. S. Nair, C. T. Laurencin, D. Gazit and C. Ortiz, *J. Biomech.*, 2007, **40**, 399–411.
12 Z. Peng, J. Gong and H. Miao, *J. Eur. Ceram. Soc.*, 2004, **24**, 2193–2201.
13 P. S. Uskokovic, C. Y. Tang, C. P. Tsui, N. Ignjatovic and D. P. Uskokovic, *J. Eur. Ceramic Soc.*, 2007, **27**, 1559–1564.
14 N. Almqvist, R. Bhatia, G. Primbs, N. Desai, S. Banerjee and R. Lal, *Biophys. J.*, 2004, **86**, 1753–1762.
15 C. Rotsch, F. Braet, E. Wisse and M. Radmacher, *Cell Biol. Int.*, 1997, **21**, 685–696.
16 A. J. Jin, K. Prasad, P. D. Smith, E. M. Lafer and R. Nossal, *Biophys. J.*, 2006, **90**, 3333–3344.
17 V. Breedveld and D. J. Pine, *J. Mater. Sci.*, 2003, **38**, 4461–4470.
18 S. Brocchini, *Adv. Drug Delivery Rev.*, 2001, **53**, 123–130.
19 J. R. Smith, A. Seyda, N. Weber, D. Knight, S. Abramson and J. Kohn, *Macromol. Rapid Commun.*, 2004, **25**, 127–140.
20 E. K. Dimitriadis, F. Horkay, J. Maresca, B. Kachar and R. S. Chadwick, *Biophys. J.*, 2002, **82**, 2798–2810.
21 H. Hertz, *J. Reine Angew. Math.*, 1881, **5**, 12–23.
22 K. L. Johnson, *Contact Mechanics*, Cambridge University Press, Cambridge, 1985.
23 J. Boussinesq, *Applications des Potentiels a l'Etude de l'Equilibre et du Mouvement des Solides Elastiques*, Gauthier-Villars, Paris, 1885.
24 A. E. H. Love, *Q. J. Math.*, 1939, **10**, 161–175.
25 C. M. Segedin, *Mathematika*, 1957, **4**, 156–161.
26 L. D. Landau and E. M. Lifshitz, *Theory of Elasticity*, Pergamon Press, Oxford, 1959.
27 I. N. Sneddon, *Int. J. Eng. Sci.*, 1965, **3**, 47–57.
28 G. Bilodeau, *J. Appl. Mech.*, 1992, **59**, 519–523.
29 F. Rico, P. Roca-Cusachs, N. Gavara, R. Farre, M. Rotger and D. Navajas, *Phys. Rev. E: Stat. Phys., Plasmas, Fluids, Relat. Interdiscip. Top.*, 2005, 72, 021914.
30 K. D. Costa and F. C. P. Yin, *J. Biomech. Eng.*, 1999, **121**, 462–471.
31 S. Na, Z. Sun, G. A. Meininger and J. D. Humphrey, *Biomech. Model. Mechanobiol.*, 2004, **3**, 75–84.
32 K. L. Johnson, K. Kendall and A. D. Roberts, *Proc. R. Soc. London, Ser. A*, 1971, **324**, 301–313.
33 B. V. Derjaguin, V. M. Muller and Y. P. Toporov, *J. Colloid Interface Sci.*, 1975, **53**, 314–326.
34 K. L. Johnson and J. A. Greenwood, *J. Colloid Interface Sci.*, 1997, **192**, 326–333.
35 D. Tabor, *J. Colloid Interface Sci.*, 1976, **58**, 2–13.
36 D. Maugis, *J. Colloid Interface Sci.*, 1992, **150**, 243–269.
37 O. Pietrement and M. Troyon, *J. Colloid Interface Sci.*, 2000, **226**, 166–171.
38 R. W. Carpick, D. F. Ogletree and M. Salmeron, *J. Colloid Interface Sci.*, 1999, **211**, 395–400.
39 Y. Sun, B. Akhremitchev and G. C. Walker, *Langmuir*, 2004, **20**, 5837–5845.
40 R. S. Chadwick, *SIAM J. Appl. Math.*, 2002, **62**, 1520–1530.

41 H. Butt, *Biophys. J.*, 1991, **60**, 1438–1444.
42 H. Butt, *Biophys. J.*, 1992, **63**, 578–582.
43 H. Butt, M. Kappl, H. Mueller and R. Raiteri, *Langmuir*, 1999, **15**, 2559–2565.
44 D. J. Johnson, N. J. Miles and N. Hilal, *Adv Colloid Interface Sci*, 2006, **127**, 67–81.
45 S. Zhong, H. Li, X. Y. Chen, E. H. Cao, G. Jin and K. S. Hu, *Langmuir*, 2007, **23**, 4486–4493.
46 T. A. Camesano and B. E. Logan, *Environ. Sci. Technol.*, 2000, **34**, 3354–3362.
47 R. J. Emerson and T. A. Camesano, *Appl. Environ. Microbiol.*, 2004, **70**, 6012–6022.
48 M. B. Salerno, X. Li and B. E. Logan, *Colloids Surf., B*, 2007, **59**, 46–51.
49 X. Sheng, Y. P. Ting and S. O. Pehkonen, *J. Colloid Interface Sci.*, 2007, **310**, 661–669.
50 D. C. Lin, E. K. Dimitriadis and F. Horkay, in *Recent Research Developments in Biophysics*, ed. S. G. Pandalai, Transworld Research Network, Kerala, India, 2006, vol. 5 Part II, pp. 333–370.
51 M. M. Gibbons and W. S. Klug, *Phys. Rev. E: Stat. Phys., Plasmas, Fluids, Relat. Interdiscip. Top.*, 2007, **75**, 031901.
52 Z. Guo and L. J. Sluys, *Int. J. Solids Struc.*, 2006, **43**, 2799–2819.
53 L. R. G. Treloar, *The Physics of Rubber Elasticity*, 3rd edn., Oxford University Press, Oxford, 1975.
54 M. McElfresh, E. Baesu, R. Balhorn, J. Belak, M. J. Allen and R. E. Rudd, *Proc. Natl. Acad. Sci. U. S. A.*, 2002, **99**, 6493–6497.
55 G. U. Unnikrishnan, V. U. Unnikrishnan and J. N. Reddy, *J. Biomech. Eng.*, 2007, **129**, 315–323.
56 M. J. Jaasma, W. M. Jackson and T. M. Keaveny, *Ann. Biomed. Eng.*, 2006, **34**, 748–758.
57 K. D. Costa, A. J. Sim and F. C. Yin, *J. Biomech. Eng.*, 2006, **128**, 176–184.
58 A. B. Mathur, A. M. Collinsworth, W. M. Reichert, W. E. Kraus and G. A. Truskey, *J. Biomech.*, 2001, **34**, 1545–1553.
59 D. C. Lin, E. K. Dimitriadis and F. Horkay, *eXPRESS Polym. Lett.*, 2007, **1**, 576–584.
60 D. C. Lin, E. K. Dimitriadis and F. Horkay, *Proceedings of the MRS Fall Meeting, Boston*, 2007.
61 D. C. Lin, D. I. Shreiber, E. K. Dimitriadis and F. Horkay, unpublished work.
62 S. L. Crick and F. C. Yin, *Biomech. Model. Mechanobiol.*, 2007, **6**, 199–210.
63 D. C. Lin, E. K. Dimitriadis and F. Horkay, *J. Biomech. Eng.*, 2007, **129**, 430–440.
64 R. Dong, T. W. Jensen, K. Engberg, R. G. Nuzzo and D. E. Leckband, *Langmuir*, 2007, **23**, 1483–1488.
65 H. Haga, S. Sasaki, K. Kawabata, E. Ito, T. Ushiki and T. Sambongi, *Ultramicroscopy*, 2000, **82**, 253–258.
66 Y. Jiao and T. E. Schaffer, *Langmuir*, 2004, **20**, 10038–10045.
67 B. Shoelson, E. K. Dimitriadis, H. Cai, B. Kachar and R. S. Chadwick, *Biophys. J.*, 2004, **87**, 2768–2777.
68 A. Touhami, B. Nysten and Y. F. Dufrene, *Langmuir*, 2003, **19**, 4539–4543.
69 S. Guo and B. B. Akhremitchev, *Biomacromolecules*, 2006, **7**, 1630–1636.
70 This is equivalent to the transformation used in Table 3, with C being similar to w_0 and Δ similar to w.
71 W. C. Oliver and G. M. Pharr, *J. Mater. Res.*, 1992, **7**, 1564–1583.
72 J. G. Jacot, S. Dianis, J. Schnall and J. Y. Wong, *J. Biomed. Mater. Res. A*, 2006, **79**, 485–494.
73 K. D. Jandt, *Surf. Sci.*, 2001, **491**, 303–332.
74 M. Stolz, R. Raiteri, A. U. Daniels, M. R. VanLandingham, W. Baschong and U. Aebi, *Biophys. J.*, 2004, **86**, 3269–3283.
75 D. Tranchida and S. Piccarolo, *Macromol. Rapid Commun.*, 2005, **26**, 1800–1804.
76 V. V. Tsukruk, Z. Huang, S. A. Chizhik and V. V. Gorbunov, *J. Mater. Sci.*, 1998, **33**, 4905–4909.
77 E. A-Hassan, W. F. Heinz, M. D. Antonik, N. P. D'Costa, S. Nageswaran, C. Schoenenberger and J. H. Hoh, *Biophys. J.*, 1998, **74**, 1564–1578.
78 L. R. Nyland and D. W. Maughan, *Biophys. J.*, 2000, **78**, 1490–1497.
79 M. Radmacher, *Methods Cell Biol.*, 2002, **68**, 67–90.
80 Y. M. Kolambkar, Master's thesis, University of Cincinnati, 2004.
81 D. C. Lin, E. K. Dimitriadis and F. Horkay, *J. Biomech. Eng.*, 2007, **129**, 904–912.
82 S. Sen, S. Subramanian and D. E. Discher, *Biophys. J.*, 2005, **89**, 3203–3213.

